Chemical Science

ROYAL SOCIETY OF CHEMISTRY

EDGE ARTICLE

View Article Online
View Journal | View Issue

Cite this: *Chem. Sci.*, 2025, **16**, 22424

All publication charges for this article have been paid for by the Royal Society of Chemistry

Received 11th August 2025
Accepted 16th October 2025

DOI: 10.1039/d5sc06069a

rsc.li/chemical-science

Narrowing emission spectra based on indolocarbazole molecular model system: an experimental and theoretical study

Yingbo Lv, Jingzhuo Bi, Runting Wang, Zhiqiang Yang, Xinqi Yang, Shuaiqiang Zhao, Shiyin Wang, Haichao Liu, Shi-Tong Zhang * and Bing Yang *

To clarify the structure–property relationship of the narrowed emission spectrum, four indolocarbazole (IDCz) model compounds were designed and synthesized. Their π-conjugated plane size can be adjusted by gradually chemically locking the benzene ring. With increasing π-conjugated plane, both 0-1 and 0-2 vibronic peaks are suppressed significantly, demonstrating a gradual narrowing of the emission spectrum. Theoretical calculations reveal that the vibronic coupling gradually weakens with the increase in π-conjugated plane, arising from the significant reduction in the number of involved vibration modes in both high-frequency and low-frequency regions. Additionally, the n → π* transition reduces the charge variation on the benzene rings, which is then diluted as the number of locked benzene rings increases. These two main factors jointly suppress the geometric changes in locked benzene rings, particularly the stretching vibrations of C–C/C=C bonds, resulting in a narrowing of the emission spectrum. This work not only helps to better understand the mechanism of narrowing the emission spectrum but also guides the molecular design of high-color-purity luminescent materials.

Introduction

As a new-generation display and lighting technology, organic light-emitting diodes (OLEDs) have received tremendous attention in recent decades.[1] To meet the increasing demands of ultra-high definition display, organic luminescent materials must have a narrow full width at half maximum (FWHM) in their emission spectra to achieve high color-purity (*e.g.*, BT 2020).[2] However, due to their inherent strong vibronic coupling, organic π-conjugated molecules typically exhibit a larger FWHM of the emission spectrum[3,4] compared to inorganic luminescent materials, such as gallium nitrides, quantum dots, rare earths, or perovskites.[5–16] To achieve a high color purity in OLEDs, additional color filters or optical cavities must be integrated into each display pixel, which not only causes a loss of some luminescent energy but also increases the cost of the product.[17] Therefore, it is of great significance to develop organic luminescent materials with narrow FWHM emissions for advanced ultra-high definition displays. However, due to the complexity and diversity of vibronic coupling in organic molecular systems, it is very challenging to design pure organic materials with narrow FWHM luminescence emissions without the knowledge of a well-defined structure–property relationship.[18,19]

In 2016, Hatakeyama and co-workers reported a novel type of organic luminescent material with a narrow FWHM of its emission spectrum, which was named as multiple-resonance (MR) thermally-activated delayed fluorescence (TADF) material.[20] In terms of molecular structure, these materials are based on the rational combination of boron (B)/nitrogen (N) heteroatoms and benzene rings. Using the MR effects induced by the B/N heteroatoms at specific substitution sites (*ortho* and *para*), the frontier molecular orbitals (FMOs) significantly localize on alternate carbon atoms of the benzene ring. Specifically, the highest occupied molecular orbital (HOMO) is mainly localized on the electron-donating N-heteroatom and its *ortho*/*para*-carbon atoms. In contrast, the lowest unoccupied molecular orbital (LUMO) is primarily localized on the electron-withdrawing B-heteroatom and its *ortho*/*para*-carbon atoms. This MR-induced staggered atomic localization of FMOs (the spatially separated HOMO and LUMO) not only minimizes the vibronic coupling between the ground state (S_0) and the lowest singlet excited state (S_1) but also greatly reduces the energy gap (ΔE_{ST}) between the S_1 state and the lowest triplet excited state (T_1), thereby endowing the narrow FWHM and TADF emission with considerable oscillator strength. Due to the advantages of narrow FWHM and TADF emission, these materials demonstrate superior OLED performance (*e.g.*, high color purity and high efficiency) in blue,[21–41] green,[42–59] and red[60–65] three-primary-color emissions. Furthermore, to avoid the tedious synthesis of B/N systems, alternative molecular designs have been developed, such as indolocarbazole (IDCz) derivatives,[66–83]

State Key Laboratory of Supramolecular Structure and Materials, College of Chemistry, Jilin University, Changchun, 130012, P. R. China. E-mail: stzhang@jlu.edu.cn; yangbing@jlu.edu.cn

N/C=O[84–94] and N/O=S=O,[95,96] *etc.*, which have also achieved narrow FWHM emission. In the same way, these narrow TADF emissions are still attributed to the MR effect, similar to the B/N molecular system. In contrast, Ma and colleagues proposed a novel mechanism with soliton-like characteristics to achieve narrowing of the emission spectrum, inspired by cyanine dyes.[97,98] Under the induction effect of the terminal donor and acceptor groups, the middle cyanine chain shows a soliton-like electronic structure, which is characterized by uniform C–C/C=C bond lengths and balanced alternating positive/negative atomic charge distribution. Thus, the high-frequency C–C stretching vibrations can be substantially suppressed due to the approximate homogenization between C–C and C=C bonds along the cyanine chain. Undoubtedly, this effective suppression of high-frequency stretching vibrations results in narrow absorption and emission spectra in soliton-like molecular systems. Overall, these two molecular systems indeed have the typical structural features that can help understand the mechanism of narrowing the emission spectra. To further enrich the new material system, a more fundamental and universal mechanism is needed to understand the structure–property relationship, thereby guiding the innovative design of organic narrow-emission molecules.

In this work, we attempt to understand the essence of a narrow emission spectrum from the perspective of electron transitions, as it is the electron transition that causes charge redistribution and leads to the subsequent molecular geometry relaxation, known as vibronic coupling. In principle, during the electron transition process, the greater the charge variation, the more significant the geometry relaxation. In this way, the details of electron transition should be carefully analyzed, considering that they may be responsible for the essence of narrowing the emission spectrum. For instance, in polycyclic aromatic hydrocarbons (PAHs), the pure $\pi \rightarrow \pi^*$ transition of perylene dominates the electronic excitation, which usually causes significant bond length changes between the S_0 and S_1 states, corresponding to strong vibronic coupling with high-frequency C–C stretching modes.[99,100] As a result, this vibronic coupling gives rise to a clear fine structure and a large FWHM in both absorption and emission spectra, as shown in Scheme 1a. For comparison, when the N-heteroatoms are introduced into PAHs, such as in the indolocarbazole (IDCz) derivative,[101] the electronic excitation involves two types of transition configurations: $n \rightarrow \pi^*$, corresponding to the n-electron transition from N-heteroatoms to benzene ring and $\pi \rightarrow \pi^*$, corresponding to the π-electrons delocalized over the benzene ring. In this case, the $n \rightarrow \pi^*$ transition can partially replace the pure $\pi \rightarrow \pi^*$ transition in PAHs. On the one hand, the N-heteroatoms share part of the charge variation caused by electronic excitation in the form of atomic localization (almost irrelevant geometry changes), which can effectively reduce the charge variation on the benzene ring. Thus, this reduced charge variation effectively suppresses the geometry changes of the benzene ring, particularly for high-frequency C–C stretching vibrations, resulting in

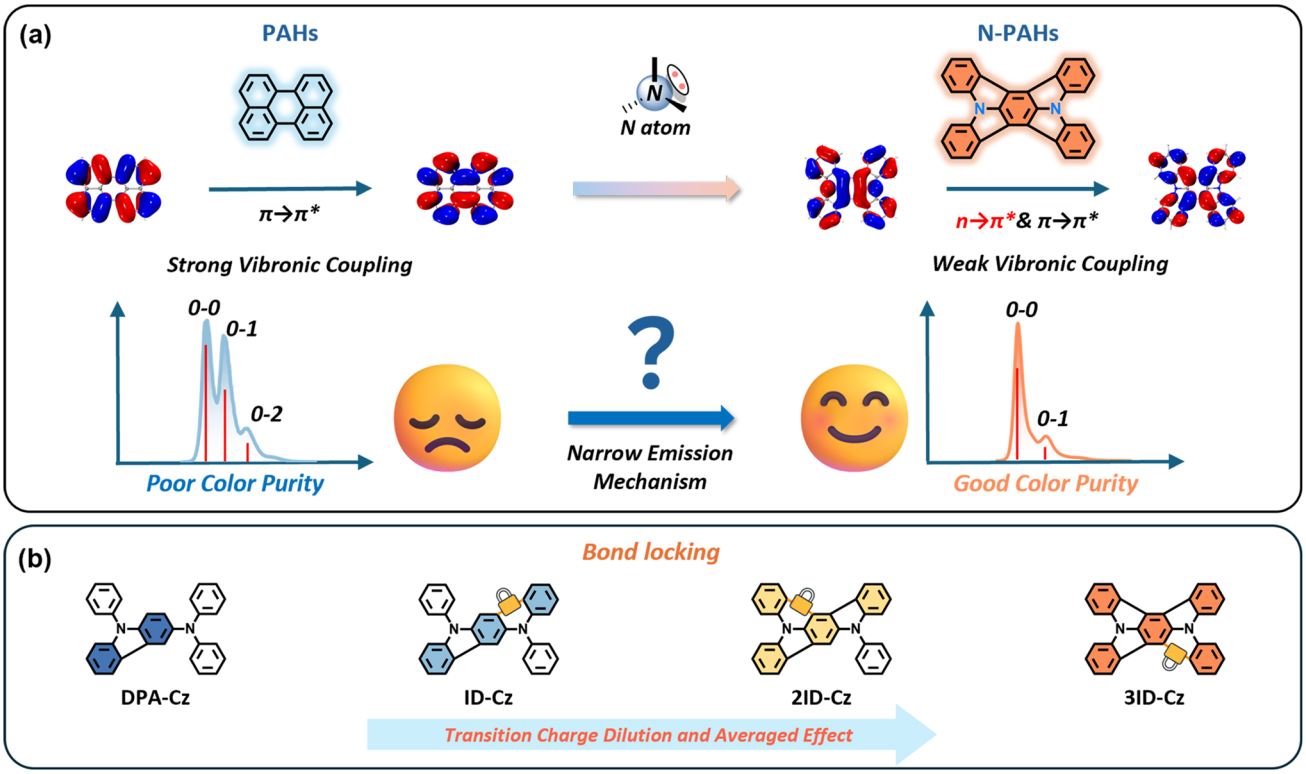

Scheme 1 (a) Schematic diagram of emission spectrum narrowing caused by $n \rightarrow \pi^*$ electron transition (from polycyclic aromatic hydrocarbons (PAHs) to nitrogen atom-containing polycyclic aromatic hydrocarbons (N-PAHs)). (b) Molecular design of four IDCz model compounds: the electron density dilution on benzene rings.

weakened vibronic coupling and a narrowed emission spectrum (Scheme 1a).

Conversely, if the charge variation on the benzene ring could be diluted, for example, by increasing the number of benzene rings, the vibronic coupling would be further suppressed, also achieving a further narrowing of the emission spectrum. To verify this idea, we designed and synthesized four model molecules (DPA-Cz, ID-Cz, 2ID-Cz, and 3ID-Cz) based on the IDCz system. Their corresponding synthetic details are depicted in Scheme S1. As shown in Scheme 1b, these four model molecules each contain two N-heteroatoms and five benzene rings, with the π-conjugated plane extended by gradually chemically locking the rotatable phenyl group. Experimental and theoretical investigations were carried out to systematically explore the evolution of their emission spectra with increasing π-conjugated plane. As expected, this IDCz model system can vividly demonstrate the emission narrowing process and mechanism, which not only contributes to a better understanding of the structure–property relationship but also provides a general strategy for the molecular design of high color-purity luminescent materials.

Results and discussion

Photophysical properties

The four model compounds were synthesized, as detailed in the SI. Their absorption and emission spectra were measured in a toluene solution (1×10^{-5} M) and are shown in Fig. 1. All of them demonstrate two main absorption bands, corresponding to the absorption of aromatic units in the short-wavelength region and the absorption of the π-conjugated molecular backbone in the long-wavelength region, respectively. Regarding the emission properties, the four compounds exhibit a red-shifted emission maximum (DPA-Cz: 408 nm, ID-Cz: 413 nm, 2ID-Cz: 429 nm, and 3ID-Cz: 444 nm) as the π-conjugated plane increases. Their photoluminescence (PL) lifetimes were determined to be 4.06 ns, 7.55 ns, 6.29 ns, and 5.69 ns, respectively. These are all assigned to the fluorescent emission characteristics, as shown in the transient photoluminescence decay curves (Fig. S2 of the SI). With increasing π-conjugated plane, their photoluminescence quantum yields (PLQYs) show a gradual increase of 7.47%, 25.35%, 36.83%, and 48.81%, respectively. For better understanding, both radiative rates (k_r) and non-radiative rates (k_{nr}) of these four compounds were estimated based on their PL lifetimes and PLQYs.[102] As a result, their gradually increased PLQYs from DPA-Cz to 3ID-Cz can be ascribed to the accelerated radiative rates (k_r) and the suppressed non-radiative rates (k_{nr}) with increasing π-conjugated plane. Interestingly, the emission spectra of these four compounds in toluene solution narrow as the π-conjugated plane increases, which corresponds to a gradually decreasing FWHM value of 44 nm, 36 nm, 33 nm, and 10 nm, respectively. In detail, except for DPA-Cz (a prominent peak at 408 nm and a shoulder at 428 nm), the other three compounds all show clear vibronic structures in their emission spectra, corresponding to three vibronic peaks (0-0, 0-1, 0-2): ID-Cz (413 nm, 420 nm, 430 nm), 2ID-Cz (429 nm, 440 nm, 450 nm), 3ID-Cz (444 nm, 450 nm, 460 nm), respectively. A summary of the photophysical properties for all four compounds in different states is provided in Tables S1–S4. Notably, the intensity ratios of vibronic subpeak (0-1) to vibronic central peak (0-0) are estimated to be 0.70, 0.63, 0.58, and 0.26 for these four compounds, respectively, indicating that the vibronic subpeaks (0-1 and 0-2) are effectively suppressed with the gradual locking of the benzene ring. Obviously, a decrease in the intensity of the subpeak (0-1) contributes to the narrowing of the emission spectrum from DPA-Cz to 3ID-Cz. In particular, 3ID-Cz exhibits the narrowest FWHM of only 10 nm in the emission spectrum, which is dominated by only the vibronic main peak (0-0), excluding the influence of other vibronic subpeaks (0-1 and 0-2). At the same time, the vibronic main peaks (0-0) of these four compounds are significantly narrowed with an increase in the π-conjugated plane, corresponding to the FWHMs of 44 nm, 14 nm, 12 nm, and 10 nm, respectively. Furthermore, to clarify the nature of the excited state, the absorption and emission spectra were measured in different solvents (hexane, ethyl ether, toluene, tetrahydrofuran, and acetonitrile). The Lippert–Mataga solvatochromic model of these compounds is provided in Fig. S4 of the SI. With the increase in solvent polarity, the redshift degree of the emission wavelengths gradually decreases from DPA-Cz to 3ID-Cz, while changes in the absorption wavelengths can almost be ignored. Among them, DPA-Cz exhibits the most obvious solvatochromic effect, accompanied by disappearing vibronic structure and spectral broadening (as shown in Fig. S1 of SI), indicating the excited state characteristic of intramolecular charge transfer (CT). In contrast, the other three compounds exhibit a weak solvatochromic effect and retain clear vibronic structures with increasing solvent polarity, which is attributable to the main characteristic of the locally excited (LE) state,

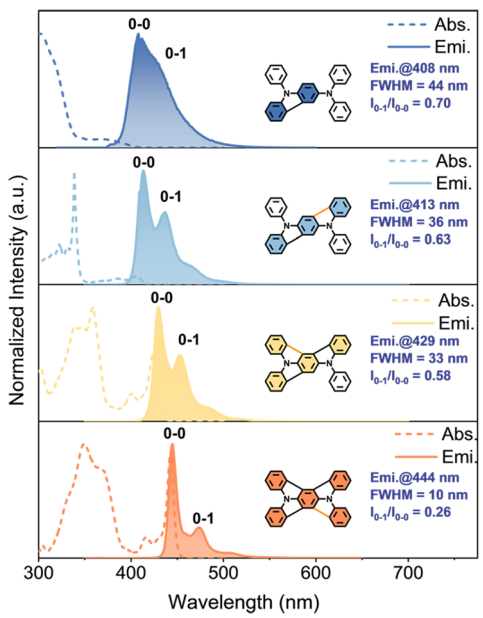

Fig. 1 UV/Vis absorption (dotted lines) and emission spectra (solid lines) of four IDCz model compounds in toluene solution (1×10^{-5} M). $I_{0\text{-}1}/I_{0\text{-}0}$ is the intensity ratio of the vibrational 0-1 peak to the central 0-0 peak.

characterized by a relatively small dipole moment. For the solid-state photophysical properties, these four compounds were doped into polymethyl methacrylate (PMMA) at a weight ratio of 1 wt% to prepare their monodisperse films, respectively. Just as in the toluene solution, the doped films also exhibit a progressively narrowed emission spectrum with increasing π-conjugated plane, together with a similar changing trend in other photophysical properties (Fig. S8 and S9). Overall, these four compounds are indeed ideal model molecules for studying the behavior and mechanism of emission spectrum narrowing, which aligns well with our molecular design goals.

Theoretical analysis

To better understand the mechanism of emission spectrum narrowing, density functional theory (DFT) and time-dependent DFT calculations were performed at the 6-31G(d,p) level for these four model molecules using the Gaussian 16 (version A.03) package.[103] For the sake of accuracy, several different functionals (O3LYP, B3LYP, PBE0, and M062X) were used in the calculations. Findings were compared with the experimental results. Theoretical results for B3LYP are in the best agreement with the experimental emission wavelengths of these four molecules (the calculation results are listed in Table S5 of SI), so subsequent calculations were carried out at the level of B3LYP/6-31G(d,p). First, their ground-state (S_0) and excited-state (S_1) geometries were optimized, respectively, as demonstrated in Fig. 2a and Tables S7–S10. From DPA-Cz to 3ID-Cz, the molecular π-conjugated plane is gradually enlarged in both S_0 and S_1 states as the number of locked benzene rings increases. Correspondingly, their reorganization energies (λ) significantly decrease with increasing π-conjugated plane along the electron (de)excitations of $S_0 \rightarrow S_1$ and $S_1 \rightarrow S_0$, respectively, indicating the gradual enhancement of molecular rigidity. Then, the frontier molecular orbitals (FMOs) and electronic energy levels of these four model molecules were calculated in the S_0 state, as shown in Fig. 2b.[104] For DPA-Cz, the highest occupied molecular orbital (HOMO) is distributed across both the carbazole and diphenylamine groups. In contrast, the lowest unoccupied molecular orbital (LUMO) is predominantly localized on the carbazole group, indicative of obvious intramolecular CT characteristics. In contrast, for the other three molecules (ID-Cz, 2ID-Cz, and 3ID-Cz), the HOMOs are primarily delocalized over the N-heteroatoms and the locked benzene rings, with a small contribution from the unlocked benzene rings. In addition, their LUMOs are almost entirely localized on the locked benzene rings, rather than on the unlocked benzene rings. With increasing π-conjugated plane, both HOMO and LUMO exhibit enhanced π-orbital delocalization and gradually stabilizing energy levels. Notably, the energy level of LUMO decreases more significantly than that of HOMO from DPA-Cz to 3ID-Cz, resulting in a reduction in the HOMO–LUMO energy gap, which is consistent with the gradual redshift of emission mentioned above.

Furthermore, the natural transition orbitals (NTOs) were calculated to analyze the electron transition properties of $S_1 \rightarrow S_0$ in these four model molecules. As shown in Fig. 3a, the hole–electron pair wavefunction reveals that the DPA-Cz molecule demonstrates obvious CT characteristics in the geometry of the

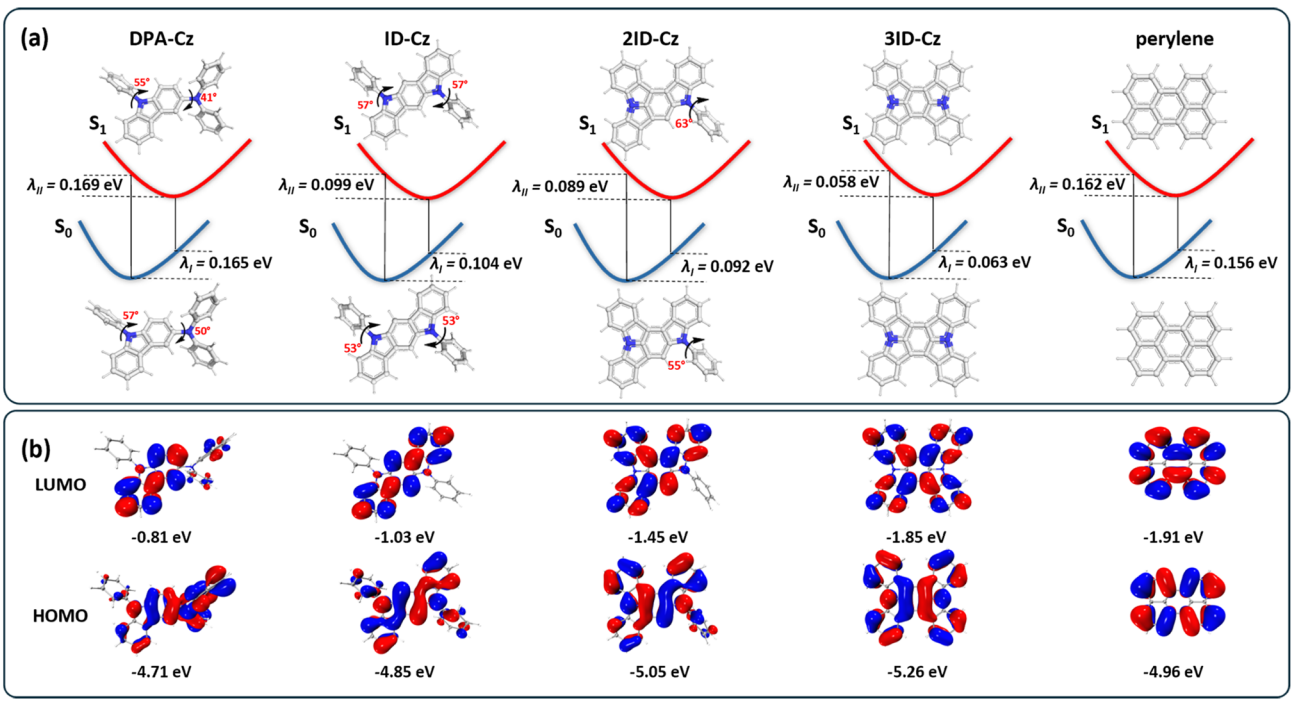

Fig. 2 (a) Optimized S_0 and S_1 geometries and reorganization energy (λ_I and λ_{II} correspond to the $S_1 \rightarrow S_0$ and $S_0 \rightarrow S_1$ transition process) of DPA-Cz, ID-Cz, 2ID-Cz, 3ID-Cz, and perylene. All of the optimized geometries were calculated using the B3LYP functional at the 6-31G (d,p) basis level. (b) Frontier molecular orbitals (HOMOs and LUMOs) and energy levels of DPA-Cz, ID-Cz, 2ID-Cz, 3ID-Cz, and perylene.

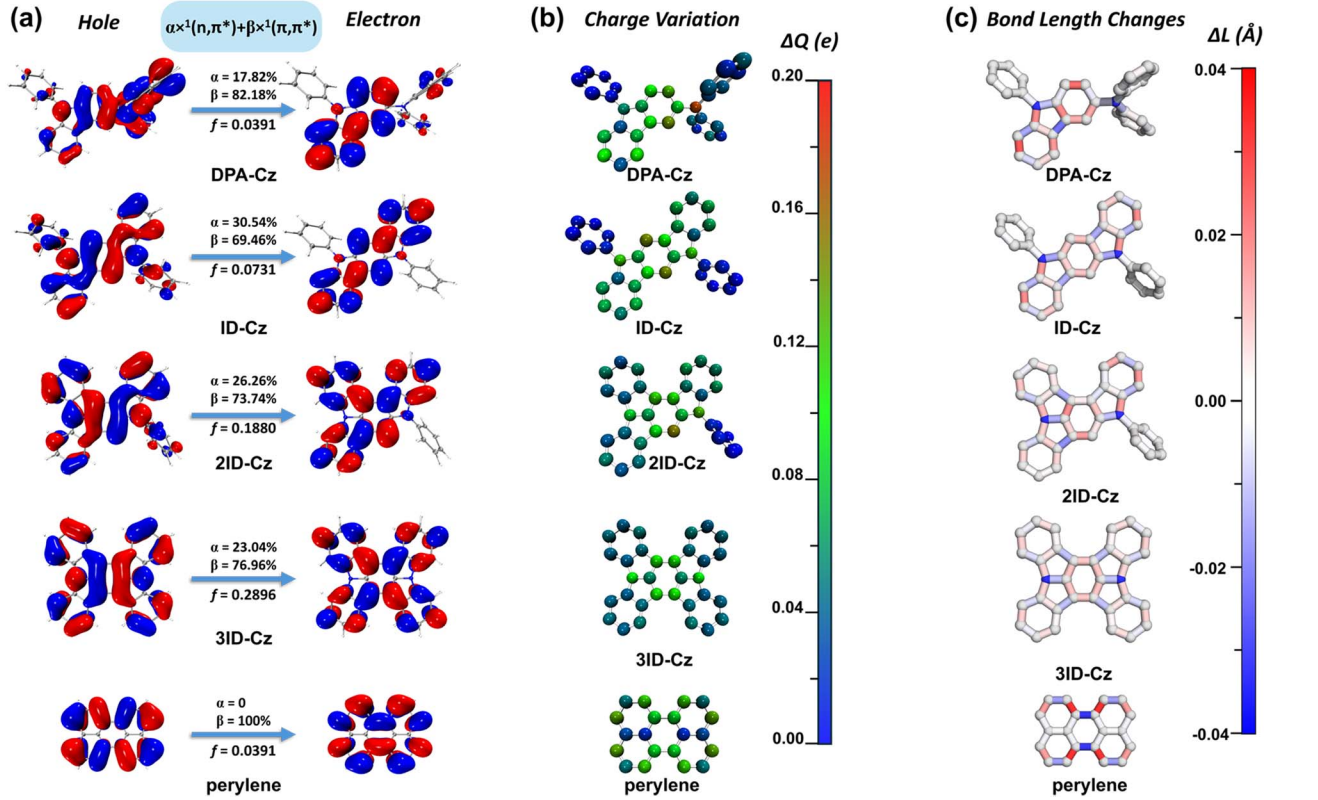

Fig. 3 (a) The NTOs of DPA-Cz, ID-Cz, 2ID-Cz, 3ID-Cz and perylene; (b) the charge variation (Δ*Q*) on each atoms of DPA-Cz, ID-Cz, 2ID-Cz, 3ID-Cz and perylene; (c) the bond length changes (Δ*L*) between ground state (S_0) and excited state (S_1) of DPA-Cz, ID-Cz, 2ID-Cz, 3ID-Cz and perylene (the red color represents the elongation of bond length, while the blue color denotes the shortening of bond length, and the color depth is proportional to the magnitude of bond length change).

S_1 state, with the wavefunction shifting from the diphenylamine group to the carbazole unit. This result agrees well with the significant solvatochromic effect observed in the experiment. Comparatively, the ID-Cz, 2ID-Cz, and 3ID-Cz predominantly exhibit LE excited state characteristics, as the vast majority of electronic transitions are concentrated in the rigid planar part of the molecules. This localization coincides with the minimal solvatochromic effect in the experiment in Fig. S1. Based on the NTOs, electronic transition properties can be identified for these four model molecules. Fig. 3a indicates that the incorporation of N-heteroatoms alters the characteristics of the electronic transition from a pure π → π* transition of perylene, a typical characteristic in PAHs, to a mixed transition with both n → π* and π → π* components. In four model molecules, the π → π* transition involves the electron transition between π and π* orbitals of benzene rings. In contrast, the n → π* transition corresponds to the electron transition of lone pair electrons (n-electrons) from the N-heteroatoms to the π* orbital of benzene rings. To quantify the actual contribution of the n → π* transition, the electronic transition composition of the S_1 → S_0 in the four model molecules was analysed by using the interfragment charge transfer (IFCT) method.[105–107] For simplicity, each model molecule is divided into three main fragments: *frag-1* and *frag-2* represent two N-heteroatoms. In addition, *frag-3* contains all the carbon (C) and hydrogen (H) atoms of the benzene rings in each molecule (Tables S11–S14). Thus, the electronic de-excitation between S_1 and S_0 states can be approximated as the electron transition among these three fragments. According to the results of IFCT calculation, the n-electron orbitals of the two N-heteroatoms contribute a certain percentage to the hole wavefunction, corresponding to 23.53% of DPA-Cz, 24.08% of ID-Cz, 20.45% of 2ID-Cz, and 18.02% of 3ID-Cz, respectively. At the same time, natural atomic orbitals (NAO) calculations show that the contribution of the n → π* transition is 17.82%, 30.54%, 26.26% and 23.04%, respectively, for the four compounds.[108] Apart from the contribution of the n → π* transition, the remaining percentages are attributed to the π → π* transition, which is limited to the benzene rings and accounts for 82.18% of DPA-Cz, 69.46% of ID-Cz, 73.74% of 2ID-Cz, and 76.96% of 3ID-Cz, respectively. It is worth noting that the lone pair n-electron in the hole wavefunction is confined to the two N-heteroatoms themselves and rarely delocalizes to adjacent atoms. Presumably, the reduction of electron density caused by the n → π* transition is also localized on the N-heteroatoms, unlike the typical π → π* transition of perylene, where the electron density change is delocalized on the π-conjugated molecular skeleton, especially between C–C and C=C bonds. As a result, the heteroatom-based localization of charge variation will result in a negligible geometry change during the S_1 → S_0, corresponding to the

minimized vibronic coupling and a narrowed emission spectrum. To verify this hypothesis, the charge redistribution of these four molecules was calculated upon the electronic excitation between S_1 and S_0 states. This result reveals a negative net variation in charge population on the two N-heteroatoms: $-0.22e$ for DPA-Cz, $-0.23e$ for ID-Cz, $-0.19e$ for 2ID-Cz, and $-0.17e$ for 3ID-Cz, respectively. To maintain electrical neutrality, the remaining five benzene rings of each compound exhibit a positive charge variation in an equal amount. For analytical simplicity, both charge gain and loss (positive and negative variations) are uniformly regarded as positive contributions, as the magnitude of charge variation, rather than its sign, directly correlates with the degree of geometry relaxation in these molecules. Additionally, we used the same calculation method to assess the charge variation of perylene. The detailed charge variation on each atom of these compounds is summarized in Tables S15–S19 of the SI. As illustrated in Fig. 3b, charge variation (ΔQ) predominantly occurs on the rigid planar part of the molecules. Obviously, charge variation in the unlocked benzene ring can be almost ignored in the first three molecules, except for the two on the diphenylamine in DPA-Cz. With an increase in the π-conjugated plane, the charge variation gradually concentrates on the central benzene ring and the two N-heteroatoms, demonstrating a decreasing trend. Notably, charge variation on the peripheral locked benzene rings is also gradually diminished. This trend is manifested not only in the reduction of the total charge variation on the locked benzene rings as estimated by the IFCT method but also in the decrease of the average charge variation on each peripheral locked benzene ring, as a result of the increase in the number of locked benzene rings. To establish the correlation between charge variations and geometry changes, the bond length changes of the C–C and C–N bonds were calculated between the S_1 and S_0 states; these are listed in Tables S20–S24 and Fig. S12. As depicted in Fig. 3c,[109] consistent with the charge redistribution pattern, the changes in bond length primarily occur in the rigid, planar part of the molecules. In contrast, changes of bond length in the unlocked benzene rings are almost negligible. With increasing π-conjugated plane, both the central and peripheral locked benzene rings show reduced fluctuations in bond lengths, and significant bond length changes gradually move toward the central benzene ring and the covalent bonds related to the two N-heteroatoms in 3ID-Cz. Compared with 3ID-Cz, the rigid perylene also shows greater charge variation and larger bond length change upon electronic excitation, which may be due to the absence of n → π* transition. In addition, it is noteworthy that the four carbon atoms on the horizontal symmetry axis of perylene do not undergo electronic excitation and exhibit almost no charge variation, which corresponds well with the unchanged bond length. This further confirms the correlation between charge variation and geometry change. These findings demonstrate the synchronous direct proportion relationship between charge variation and geometry relaxation, which vividly reveals the essence of vibronic coupling. The geometry changes are caused by charge redistribution upon electron (de)excitation.

Moreover, the vibronic coupling was quantitatively calculated to understand the formation of the vibronic fine structures and the nature of the narrowing emission spectrum. For this purpose, the reorganization energy and Huang–Rhys (HR) factors of these four model molecules and perylene were calculated, and their vibronically resolved emission spectra were simulated using the MOMAP package.[110–112] As shown in Fig. 4a, the reorganization energy of the four molecules is given for all active vibration modes. Overall, with an increase in the locked benzene rings, both the total reorganization energy and the active vibration modes significantly decrease, indicating that vibronic coupling is greatly weakened from DPA-Cz to 3ID-Cz. Although the low-frequency vibration modes exhibit a larger HR factor than the high-frequency modes (Fig. S13), they generally contribute very little to the reorganization energy and the broadening of the emission spectrum, because they have a smaller vibrational energy than the high-frequency ones. On the contrary, the high-frequency vibronic coupling is generally responsible for the generation of vibronic fine structures, resulting in a substantial broadening of the emission spectrum. For a clear comparison, the high-frequency region is highlighted in the range of 1200–1700 cm^{-1}, as shown in Fig. 4a. Importantly, in this region, two main categories of vibration modes contribute to the vibronic coupling: (1) the combined vibration of C–N and C–C stretching based on the central benzene ring (1200–1500 cm^{-1}), and (2) the C–C stretching vibration of the peripheral benzene ring (1500–1700 cm^{-1}).[99,113] For ease of understanding, the major-contribution vibration modes in both low-frequency and high-frequency regions are illustrated in Fig. 4a, which primarily contribute to the vibronic coupling in these molecules.

Meanwhile, their vibronically resolved emission spectra are theoretically simulated, as shown in Fig. 4b. The simulated emission spectra are all in good agreement with the experimental fluorescence spectra, especially for the vibronic fine structures, which well verifies the reliability of the whole calculations. Obviously, the 0-0 vibronic main peak of the emission spectrum is affected by the low-frequency vibration modes, while the other vibronic fine peaks can be ascribed to the contribution of high-frequency vibration modes, especially for the 0-1 peak in this molecular series. In contrast, DPA-Cz exhibits the most ambiguous vibronic fine structure and the broadest emission spectrum, resulting from the strongest vibronic coupling in both low-frequency and high-frequency regions among these four model molecules. With the expansion of π-conjugated plane, the vibronic coupling in both low-frequency and high-frequency regions significantly decreases, resulting in the gradual narrowing of the simulated emission spectrum from ID-Cz to 3ID-Cz. Notably, the two main types of high-frequency vibration modes contribute to the intensity of the 0-1 peak in the simulated emission spectrum, corresponding to the combined vibration of C–N and C–C stretching based on the central benzene ring (1200–1500 cm^{-1}) and the C–C stretching vibration of the peripheral benzene ring (1500–1700 cm^{-1}), respectively.[99,114] Overall, their piecewise sums of reorganization energy are also obviously decreased with an increase in the π-conjugated plane (Fig. 4c and Table S25),

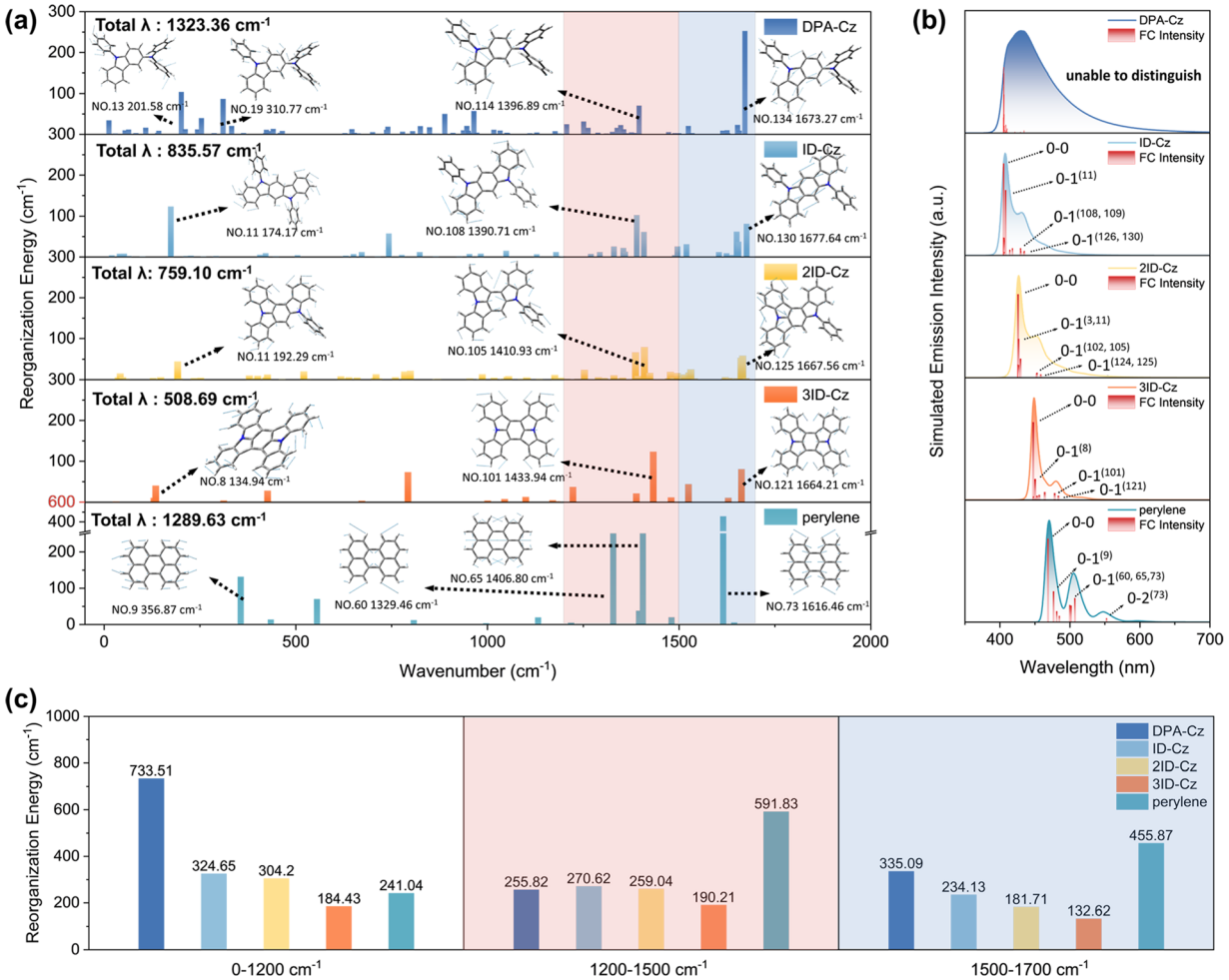

Fig. 4 (a) Reorganization energy *versus* normal-mode frequency at the S_0 potential energy surface, and the high-frequency region is highlighted in the range of 1200–1700 cm^{-1} for clarity. (b) Simulated vibronically resolved emissions spectra of DPA-Cz, ID-Cz, 2ID-Cz, 3ID-Cz, and perylene. (c) The total λ in 0–1200 cm^{-1} (white background), 1200–1500 cm^{-1} (red background) and 1500–1700 cm^{-1} (blue background) frequency region.

which facilitates the suppression of the 0-1 fine peak from ID-Cz to 3ID-Cz, resulting in a gradually narrowing emission spectrum. Notably, these main-contribution vibration modes align with the most significant geometry change between the S_1 and S_0 states, which also corresponds to the region of maximum charge variation induced by electronic excitation. For instance, the C–N and C–C stretching vibrations based on the central benzene ring (1433 cm^{-1}) contribute the largest reorganization energy in 3ID-Cz, coinciding with the most significant charge variation on the two N-heteroatoms and central benzene ring during the electronic excitation. At the same time, the reorganization energy contributed by the C–C stretching vibrations (1500–1700 cm^{-1}) significantly decreases from DPA-Cz to 3ID-Cz, corresponding to the effective suppression of high-frequency vibronic coupling from peripheral locked benzene rings. The reason is that, with an increase in the number of locked benzene rings, their charge variations decrease and average due to electron delocalization and the dilution effect, resulting in smaller bond length changes in the peripheral locked benzene rings, as mentioned above. In comparison, the rigid perylene exhibits a much broader emission spectrum (higher 0-1 and 0-2 fine peaks) than 3ID-Cz, resulting from the stronger vibronic coupling (larger reorganization energy) of perylene in both low-frequency and high-frequency regions. This suggests that the narrowing of the emission spectrum is not feasible solely through the planar rigid PAHs with the $\pi \rightarrow \pi^*$ transition, while heteroatom embedding is necessary to form the $n \rightarrow \pi^*$ transition. All of the mentioned main vibration modes in each frequency range of these compounds are listed in Fig. S14–S18 and Tables S26–S30 of the SI.

Overall, the mechanism of the emission spectrum narrowing in the IDCz molecular system can be clarified, as shown in Fig. 5. On the one hand, the introduction of N-heteroatoms induces the $n \rightarrow \pi^*$ transition from the N-heteroatoms to the benzene rings, which partially replaces the pure $\pi \rightarrow \pi^*$ transition in PAH molecules. Due to the atom-based localization of n-orbital, the $n \rightarrow \pi^*$ transition substantially reduces charge variations on the benzene rings upon electronic excitation, especially between C–C and C=C bonds of the benzene ring. Thus, the less the charge variation, the smaller the geometry

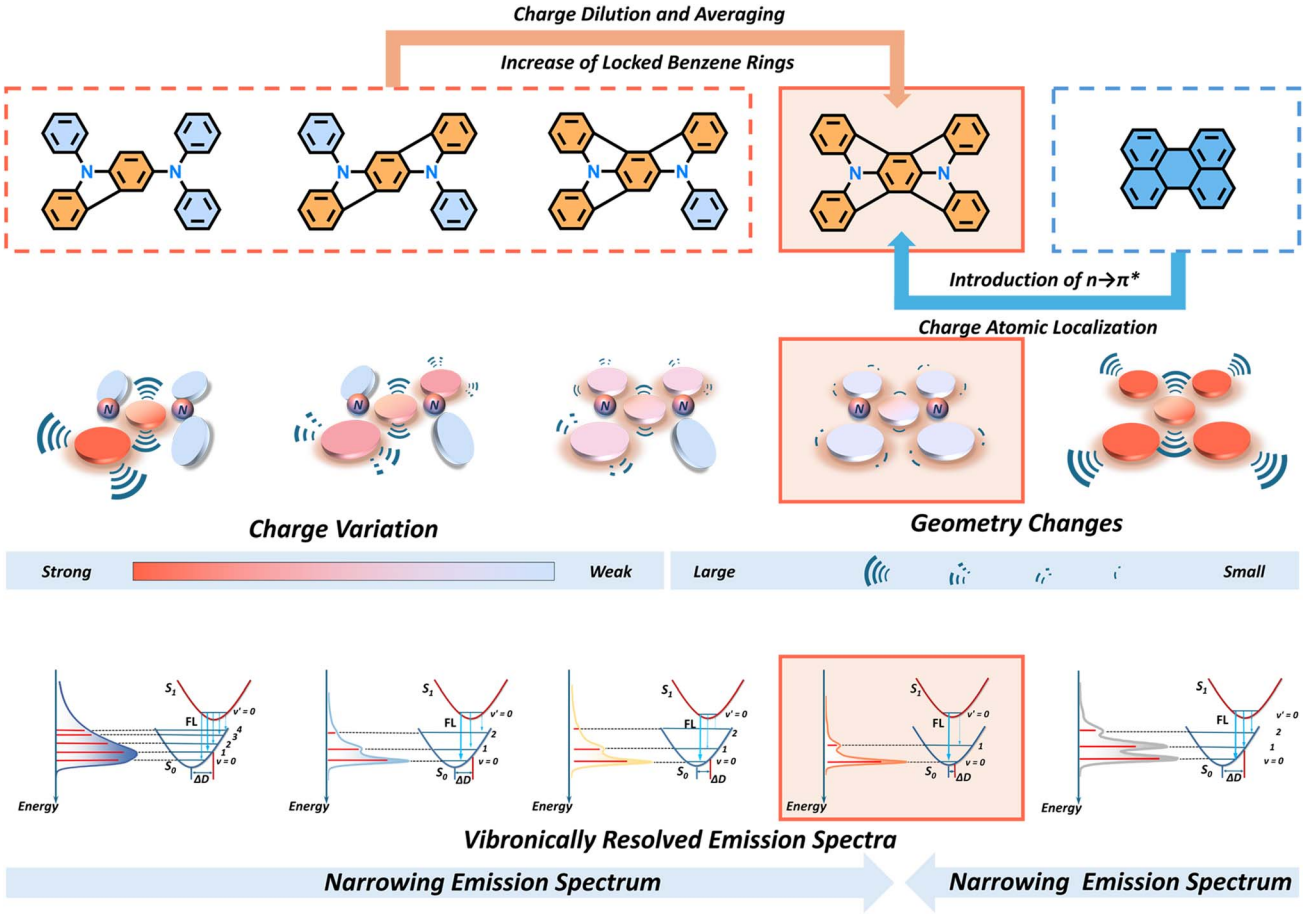

Fig. 5 Mechanism of emission spectrum narrowing.

change (ΔD), which corresponds to a decrease in reorganization energy and vibronic coupling. Meanwhile, as the number of peripheral benzene rings increases, the charge variations on the benzene rings are significantly diluted and averaged upon electronic excitation. This dilution effect also leads to the obviously reduced geometry changes (ΔD), especially on the peripheral locked benzene rings. With increasing π-conjugated plane, the reorganization energy decreases significantly, corresponding to the suppressed vibronic coupling, particularly for high-frequency C–C stretching vibrations on the peripheral locked benzene rings, which effectively suppresses the intensity of the 0-1 vibronic fine peak in the emission spectrum. As a result, these two factors work together to suppress the 0-1 vibronic fine peak, narrowing the emission spectrum from DPA-Cz to 3ID-Cz. Based on the above understanding, the general molecular design strategy for achieving a narrow emission spectrum can be proposed: (1) a planar rigid molecular structure with heteroatoms and benzene rings as the basic building blocks should be designed to avoid the formation of the long-range CT, due to the strong vibronic coupling caused by maximal charge variations before and after electronic excitation; (2) the heteroatoms should be selected as electron-rich (*e.g.*, N) or electron-deficient (*e.g.*, B) atoms or the combination of both, which form the n → π*, π→p_z^*(B) or n→p_z^*(B) transitions to alleviate the charge variation on benzene rings upon electronic excitation, effectively suppressing the vibronic coupling from high-frequency C–C stretching of the benzene rings; (3) the molecular symmetry needs to be taken into account to dilute the charge variation upon electronic excitation by increasing the number of benzene rings with equal status. Expectedly, this strategy can guide the design of novel molecular systems, especially beyond classic B/N systems, to achieve narrow FWHM emission with high color purity.

Conclusions

In summary, through the variable combination of two N-heteroatoms and five benzene rings, four model compounds based on indolocarbazole (IDCz) were designed and synthesized to better understand the structure–property relationship for narrowing the emission spectrum. In the experiment, the FWHM of their emission spectra gradually narrows as the π-conjugated plane increases, which is due to the suppression of the 0-1 vibronic fine peak. Theoretical calculations reveal that vibronic coupling gradually weakens with an increase in the π-conjugated plane due to the significant decrease in the number of active vibration modes in both high-frequency and low-frequency regions. Essentially, the electron transition was

analyzed to understand the vibronic coupling in these four model molecules, as the charge redistribution variation caused by electronic excitation is proportional to the change in molecular geometry. On the one hand, the introduction of N-heteroatoms forms the n → π* transition, which partially replaces the π → π* transition, leading to a reduction in the charge variations on the benzene rings; on the other hand, with an increasing number of locked benzene rings, the charge variations in the benzene rings were diluted and averaged, resulting in suppressed vibronic coupling of C–C stretching on the peripheral benzene rings and the narrowed emission spectrum. Overall, this work intuitively demonstrates the emission narrowing process based on the IDCz model system, which not only contributes to a better understanding of the structure–property relationship but also provides molecular design guidance for high-color-purity luminescent materials.

Author contributions

Conceptualization: B. Yang, S.-T. Zhang and H. Liu. Data curation: Y. Lv, R. Wang, X. Yang, S. Zhao, S. Wang and B. Yang. Chemical synthesis and product analysis: Y. Lv and J. Bi. Theoretical calculation and analysis: Y. Lv, B. Yang, and Z. Yang. Supervision: B. Yang. Funding acquisition: B. Yang, H. Liu, and S.-T. Zhang. Writing original draft: Y. Lv and B. Yang. Writing – review and editing: B. Yang, Y. Lv, and S.-T. Zhang.

Conflicts of interest

There are no conflicts to declare.

Data availability

All other data, including details on compounds synthesis methods, photophysical property characterization, and theoretical calculations, supporting the findings of this study are available within the article and its supplementary information (SI), as well as available from the corresponding authors upon reasonable request. Supplementary information is available. See DOI: https://doi.org/10.1039/d5sc06069a.

Acknowledgements

This work is supported by the National Key Research and Development Program of China (No. 2020YFA0714603), the National Natural Science Foundation of China (No. 52373183, 52103209, and 52073117), and the China Postdoctoral Science Foundation (No. 2024M761125). The authors gratefully acknowledge HZWTECH for providing computational facilities.

References

1 C. W. Tang and S. A. VanSlyke, Organic electroluminescent diodes, *Appl. Phys. Lett.*, 1987, **51**, 913–915.
2 S. Takasugi, H.-J. Shin, M.-K. Chang, S.-M. Ko, H.-J. Park, J.-P. Lee, H.-S. Kim and C.-H. Oh, Advanced compensation technologies for large-sized UHD OLED TVs, *J. Soc. Inf. Disp.*, 2016, **24**, 410–418.
3 H. Park, J. Lee, I. Kang, H. Y. Chu, J.-I. Lee, S.-K. Kwon and Y.-H. Kim, Highly rigid and twisted anthracene derivatives: a strategy for deep blue OLED materials with theoretical limit efficiency, *J. Mater. Chem.*, 2012, **22**, 2695–2700.
4 H. Jung, S. Kang, H. Lee, Y.-J. Yu, J. H. Jeong, J. Song, Y. Jeon and J. Park, High Efficiency and Long Lifetime of a Fluorescent Blue-Light Emitter Made of a Pyrene Core and Optimized Side Groups, *ACS Appl. Mater. Interfaces*, 2018, **10**, 30022–30028.
5 V. L. Colvin, M. C. Schlamp and A. P. Alivisatos, Light-emitting diodes made from cadmium selenide nanocrystals and a semiconducting polymer, *Nature*, 1994, **370**, 354–357.
6 S. Coe, W.-K. Woo, M. Bawendi and V. Bulović, Electroluminescence from single monolayers of nanocrystals in molecular organic devices, *Nature*, 2002, **420**, 800–803.
7 S.-I. Park, Y. Xiong, R.-H. Kim, P. Elvikis, M. Meitl, D.-H. Kim, J. Wu, J. Yoon, C.-J. Yu, Z. Liu, Y. Huang, K.-c. Hwang, P. Ferreira, X. Li, K. Choquette and J. A. Rogers, Printed Assemblies of Inorganic Light-Emitting Diodes for Deformable and Semitransparent Displays, *Science*, 2009, **325**, 977–981.
8 L. Protesescu, S. Yakunin, M. I. Bodnarchuk, F. Krieg, R. Caputo, C. H. Hendon, R. X. Yang, A. Walsh and M. V. Kovalenko, Nanocrystals of Cesium Lead Halide Perovskites (CsPbX3, X = Cl, Br, and I): Novel Optoelectronic Materials Showing Bright Emission with Wide Color Gamut, *Nano Lett.*, 2015, **15**, 3692–3696.
9 Y. Yang, Y. Zheng, W. Cao, A. Titov, J. Hyvonen, J. R. Manders, J. Xue, P. H. Holloway and L. Qian, High-efficiency light-emitting devices based on quantum dots with tailored nanostructures, *Nat. Photonics*, 2015, **9**, 259–266.
10 R. Zhu, Z. Luo, H. Chen, Y. Dong and S.-T. Wu, Realizing Rec. 2020 color gamut with quantum dot displays, *Opt. Express*, 2015, **23**, 23680–23693.
11 R. S. Cok, M. Meitl, R. Rotzoll, G. Melnik, A. Fecioru, A. J. Trindade, B. Raymond, S. Bonafede, D. Gomez, T. Moore, C. Prevatte, E. Radauscher, S. Goodwin, P. Hines and C. A. Bower, Inorganic light-emitting diode displays using micro-transfer printing, *J. Soc. Inf. Disp.*, 2017, **25**, 589–609.
12 X. Dai, Y. Deng, X. Peng and Y. Jin, Quantum-Dot Light-Emitting Diodes for Large-Area Displays: Towards the Dawn of Commercialization, *Adv. Mater.*, 2017, **29**, 1607022.
13 S. Kumar, J. Jagielski, N. Kallikounis, Y.-H. Kim, C. Wolf, F. Jenny, T. Tian, C. J. Hofer, Y.-C. Chiu, W. J. Stark, T.-W. Lee and C.-J. Shih, Ultrapure Green Light-Emitting Diodes Using Two-Dimensional Formamidinium Perovskites: Achieving Recommendation 2020 Color Coordinates, *Nano Lett.*, 2017, **17**, 5277–5284.
14 K. Zhang, D. Peng, K. M. Lau and Z. Liu, Fully-integrated active matrix programmable UV and blue micro-LED

display system-on-panel (SoP), *J. Soc. Inf. Disp.*, 2017, **25**, 240–248.

15 D. Yu, F. Cao, Y. Gao, Y. Xiong and H. Zeng, Room-Temperature Ion-Exchange-Mediated Self-Assembly toward Formamidinium Perovskite Nanoplates with Finely Tunable, Ultrapure Green Emissions for Achieving Rec. 2020 Displays, *Adv. Funct. Mater.*, 2018, **28**, 1800248.

16 Q. Zhang, X. Sun, W. Zheng, Q. Wan, M. Liu, X. Liao, T. Hagio, R. Ichino, L. Kong, H. Wang and L. Li, Band Gap Engineering toward Wavelength Tunable CsPbBr3 Nanocrystals for Achieving Rec. 2020 Displays, *Chem. Mater.*, 2021, **33**, 3575–3584.

17 T.-Y. Cho, C.-L. Lin and C.-C. Wu, Microcavity two-unit tandem organic light-emitting devices having a high efficiency, *Appl. Phys. Lett.*, 2006, **88**, 111106.

18 J. Kang, D. J. Shin and J. Y. Lee, Recent Advances in Narrow Emission Bandwidth Materials for Application in Organic Light-Emitting Diodes, *Adv. Opt. Mater.*, 2025, **13**, 2402653.

19 X. Wu, S. Ni, C.-H. Wang, W. Zhu and P.-T. Chou, Comprehensive Review on the Structural Diversity and Versatility of Multi-Resonance Fluorescence Emitters: Advance, Challenges, and Prospects toward OLEDs, *Chem. Rev.*, 2025, **125**, 6685–6752.

20 T. Hatakeyama, K. Shiren, K. Nakajima, S. Nomura, S. Nakatsuka, K. Kinoshita, J. Ni, Y. Ono and T. Ikuta, Ultrapure Blue Thermally Activated Delayed Fluorescence Molecules: Efficient HOMO-LUMO Separation by the Multiple Resonance Effect, *Adv. Mater.*, 2016, **28**, 2777–2781.

21 X. Liang, Z.-P. Yan, H.-B. Han, Z.-G. Wu, Y.-X. Zheng, H. Meng, J.-L. Zuo and W. Huang, Peripheral Amplification of Multi-Resonance Induced Thermally Activated Delayed Fluorescence for Highly Efficient OLEDs, *Angew. Chem.*, 2018, **130**, 11486–11490.

22 K. Matsui, S. Oda, K. Yoshiura, K. Nakajima, N. Yasuda and T. Hatakeyama, One-Shot Multiple Borylation toward BN-Doped Nanographenes, *J. Am. Chem. Soc.*, 2018, **140**, 1195–1198.

23 Y. Kondo, K. Yoshiura, S. Kitera, H. Nishi, S. Oda, H. Gotoh, Y. Sasada, M. Yanai and T. Hatakeyama, Narrowband deep-blue organic light-emitting diode featuring an organoboron-based emitter, *Nat. Photonics*, 2019, **13**, 678–682.

24 J. A. Knöller, G. Meng, X. Wang, D. Hall, A. Pershin, D. Beljonne, Y. Olivier, S. Laschat, E. Zysman-Colman and S. Wang, Intramolecular Borylation via Sequential B−Mes Bond Cleavage for the Divergent Synthesis of B,N,B-Doped Benzo[4]helicenes, *Angew. Chem., Int. Ed.*, 2020, **59**, 3156–3160.

25 S. M. Suresh, E. Duda, D. Hall, Z. Yao, S. Bagnich, A. M. Z. Slawin, H. Bässler, D. Beljonne, M. Buck, Y. Olivier, A. Köhler and E. Zysman-Colman, A Deep Blue B,N-Doped Heptacene Emitter That Shows Both Thermally Activated Delayed Fluorescence and Delayed Fluorescence by Triplet–Triplet Annihilation, *J. Am. Chem. Soc.*, 2020, **142**, 6588–6599.

26 M. Yang, I. S. Park and T. Yasuda, Full-Color, Narrowband, and High-Efficiency Electroluminescence from Boron and Carbazole Embedded Polycyclic Heteroaromatics, *J. Am. Chem. Soc.*, 2020, **142**, 19468–19472.

27 Y. Qiu, H. Xia, J. Miao, Z. Huang, N. Li, X. Cao, J. Han, C. Zhou, C. Zhong and C. Yang, Narrowing the Electroluminescence Spectra of Multiresonance Emitters for High-Performance Blue OLEDs by a Peripheral Decoration Strategy, *ACS Appl. Mater. Interfaces*, 2021, **13**, 59035–59042.

28 J. Bian, S. Chen, L. Qiu, R. Tian, Y. Man, Y. Wang, S. Chen, J. Zhang, C. Duan, C. Han and H. Xu, Ambipolar Self-Host Functionalization Accelerates Blue Multi-Resonance Thermally Activated Delayed Fluorescence with Internal Quantum Efficiency of 100%, *Adv. Mater.*, 2022, **34**, 2110547.

29 Q. Li, Y. Wu, X. Wang, Q. Yang, J. Hu, R. Zhong, S. Shao and L. Wang, Boron-, sulfur- and nitrogen-doped polycyclic aromatic hydrocarbon multiple resonance emitters for narrowband blue emission, *Chem. Eur. J.*, 2022, **28**, e202104214.

30 X. F. Luo, H. X. Ni, H. L. Ma, Z. Z. Qu, J. Wang, Y. X. Zheng and J. L. Zuo, Fused π-Extended Multiple-Resonance Induced Thermally Activated Delayed Fluorescence Materials for High-Efficiency and Narrowband OLEDs with Low Efficiency Roll-Off, *Adv. Opt. Mater.*, 2022, **10**, 2102513.

31 I. S. Park, M. Yang, H. Shibata, N. Amanokura and T. Yasuda, Achieving Ultimate Narrowband and Ultrapure Blue Organic Light-Emitting Diodes Based on Polycyclo-Heteraborin Multi-Resonance Delayed-Fluorescence Emitters, *Adv. Mater.*, 2022, **34**, 2107951.

32 X. Wang, Y. Zhang, H. Dai, G. Li, M. Liu, G. Meng, X. Zeng, T. Huang, L. Wang, Q. Peng, D. Yang, D. Ma, D. Zhang and L. Duan, Mesityl-Functionalized Multi-Resonance Organoboron Delayed Fluorescent Frameworks with Wide-range Color Tunability for Narrowband OLEDs, *Angew. Chem., Int. Ed.*, 2022, **61**, e202206916.

33 X. Yan, Z. Li, Q. Wang, Y. Qu, Y. Xu and Y. Wang, Achieving highly efficient narrowband sky-blue electroluminescence with alleviated efficiency roll-off by molecular-structure regulation and device-configuration optimization, *J. Mater. Chem. C*, 2022, **10**, 15408–15415.

34 T. Wang, X. Yin, X. Cao and C. Yang, A Simple Approach to Solution-Processible Small-Molecule Multi-Resonance TADF Emitters for High -Performance Narrowband OLEDs, *Angew. Chem., Int. Ed.*, 2023, **62**, e202301988.

35 T. Hua, X. Cao, J. Miao, X. Yin, Z. Chen, Z. Huang and C. Yang, Deep-blue organic light-emitting diodes for ultrahigh-definition displays, *Nat. Photonics*, 2024, **18**, 1161–1169.

36 L. Wu, X. Mu, D. Liu, W. Li, D. Li, J. Zhang, C. Liu, T. Feng, Y. Wu, J. Li, S.-J. Su and Z. Ge, Regional Functionalization Molecular Design Strategy: A Key to Enhancing the Efficiency of Multi-Resonance OLEDs, *Angew. Chem., Int. Ed.*, 2024, **63**, e202409580.

37 L. Guo, W. Cui, L. Li, Y. Pu, K. Wang, P. Zheng, Y. Wang and C. Li, Synergetic Multiple Charge-Transfer Excited States for Anti-Quenching and Rapid Spin-Flip Multi-Resonance Thermally Activated Delayed Fluorescence Emitter, *Adv. Mater.*, 2025, **37**, 2500269.

38 L. Hua, H. Wu, Z. Xia, M. Li, Y. Liu, S. Yan, W. Zhu, J. Y. Lee, Z. Ren and Y. Wang, Narrowband Emissive Solution-Processed Polymer Organic Light-Emitting Diodes with External Quantum Efficiency Above 30%, *Adv. Mater.*, 2025, **37**, 2502180.

39 Y. Kitamoto, A. Ogawa, M. Inakawa, Y. Fujimoto, M. Koshimizu, K. Oda, H. Taka, H. Kita and T. Hattori, Molecular Design and Synthesis of Narrowband Near-Ultraviolet and Pure Deep-Blue Thermally Activated Delayed Fluorescence Materials by an Ether Group Strategy, *Angew. Chem., Int. Ed.*, 2025, **64**, e202510891.

40 H. Lin, Z. Ye, S. Xian, Z. Chen, J. Miao, Z. Huang, C. Zhong, S. Gong, X. Cao and C. Yang, Deep-Blue Narrowband OLEDs Achieve External Quantum Efficiency Over 40% and Blue Index of 422 by Synergistic π-Extension and Heavy-Atom Effect, *Adv. Mater.*, 2025, **37**, 2502459.

41 F. Zhan, K. Xu, T. Tsuboi, Y. She and G. Li, A High-Efficiency Ultraviolet Organic Light-Emitting Diode Employing a Double Boron–Oxygen–Nitrogen-Based Emitter, *Angew. Chem., Int. Ed.*, 2025, **64**, e202505328.

42 Y. Zhang, D. Zhang, J. Wei, Z. Liu, Y. Lu and L. Duan, Multi-Resonance Induced Thermally Activated Delayed Fluorophores for Narrowband Green OLEDs, *Angew. Chem., Int. Ed.*, 2019, **58**, 16912–16917.

43 N. Ikeda, S. Oda, R. Matsumoto, M. Yoshioka, D. Fukushima, K. Yoshiura, N. Yasuda and T. Hatakeyama, Solution-Processable Pure Green Thermally Activated Delayed Fluorescence Emitter Based on the Multiple Resonance Effect, *Adv. Mater.*, 2020, **32**, 2004072.

44 Y. Xu, Z. Cheng, Z. Li, B. Liang, J. Wang, J. Wei, Z. Zhang and Y. Wang, Molecular-Structure and Device-Configuration Optimizations toward Highly Efficient Green Electroluminescence with Narrowband Emission and High Color Purity, *Adv. Opt. Mater.*, 2020, **8**, 1902142.

45 Y. Zhang, D. Zhang, J. Wei, X. Hong, Y. Lu, D. Hu, G. Li, Z. Liu, Y. Chen and L. Duan, Achieving Pure Green Electroluminescence with CIEy of 0.69 and EQE of 28.2% from an Aza-Fused Multi-Resonance Emitter, *Angew. Chem., Int. Ed.*, 2020, **59**, 17499–17503.

46 P. Jiang, J. Miao, X. Cao, H. Xia, K. Pan, T. Hua, X. Lv, Z. Huang, Y. Zou and C. Yang, Quenching-Resistant Multiresonance TADF Emitter Realizes 40% External Quantum Efficiency in Narrowband Electroluminescence at High Doping Level, *Adv. Mater.*, 2021, **34**, 2106954.

47 X. F. Luo, H. X. Ni, A. Q. Lv, X. K. Yao, H. L. Ma and Y. X. Zheng, High-Efficiency and Narrowband OLEDs from Blue to Yellow with Ternary Boron/Nitrogen-Based Polycyclic Heteroaromatic Emitters, *Adv. Opt. Mater.*, 2022, **10**, 2200504.

48 J. Wang, J. Miao, C. Jiang, S. Luo, C. Yang and K. Li, Engineering Intramolecular π-Stacking Interactions of Through-Space Charge-Transfer TADF Emitters for Highly Efficient OLEDs with Improved Color Purity, *Adv. Opt. Mater.*, 2022, **10**, 2201071.

49 Y. Xu, C. Li, Z. Li, J. Wang, J. Xue, Q. Wang, X. Cai and Y. Wang, Highly Efficient Electroluminescent Materials with High Color Purity Based on Strong Acceptor Attachment onto B–N-Containing Multiple Resonance Frameworks, *CCS Chem.*, 2022, **4**, 2065–2079.

50 Y. Xu, Q. Wang, J. Wei, X. Peng, J. Xue, Z. Wang, S.-J. Su and Y. Wang, Constructing Organic Electroluminescent Material with Very High Color Purity and Efficiency Based on Polycyclization of Multiple Resonance Parent Core, *Angew. Chem., Int. Ed.*, 2022, **61**, e202204652.

51 K. Zhao, Z.-F. Yao, Z.-Y. Wang, J.-C. Zeng, L. Ding, M. Xiong, J.-Y. Wang and J. Pei, "Spine Surgery" of Perylene Diimides with Covalent B–N Bonds toward Electron-Deficient BN-Embedded Polycyclic Aromatic Hydrocarbons, *J. Am. Chem. Soc.*, 2022, **144**, 3091–3098.

52 X.-F. Luo, H.-X. Ni, L. Sheng, L. Wang, X. Xiao and Y.-X. Zheng, Indolo[3,2,1-jk]carbazole Fused Multiple Resonance Induced Thermally Activated Delayed Fluorescence Emitter for Efficient Narrowband OLED, *Chem. Commun.*, 2023, **59**, 2489–2492.

53 Z. Chen, Z. Li, Y. Tian, D. Liu, Z. Yang, M. Li and S.-J. Su, Narrow-Band Dibenzoselenophene-Based Emitter with Rapid Triplet Conversion for Versatile OLED Applications with Superior Roll-Off Suppression, *Angew. Chem., Int. Ed.*, 2025, **64**, e202507626.

54 X.-C. Fan, X. Tang, T.-Y. Zhang, S. Kohata, J. Yu, X.-K. Chen, K. Wang, T. Hatakeyama, C. Adachi and X.-H. Zhang, Stable narrowband blue OLEDs by modulating frontier molecular orbital levels, *Nat. Commun.*, 2025, **16**, 4936.

55 T. Huang, Y. Xu, Y. Qu, X. Lu, K. Ye, X. Zhuang and Y. Wang, Azepination-Induced Frontier Molecular Orbital Delocalization of Multiple Resonance Emitters: Constructing Highly Efficient Narrowband Electroluminescent Materials, *Adv. Mater.*, 2025, **37**, 2503383.

56 L. Li, T. Huang, Y. Xu, Y. Qu, W. Cui, L. Xu, C. Li and Y. Wang, Ultra-Narrowband Organic Electroluminescence with External Quantum Efficiency of 40% from Indolocarbazole-Embedded Multiple Resonance Emitters, *Angew. Chem., Int. Ed.*, 2025, **64**, e202504002.

57 Y. Qu, Y. Xu, T. Huang, X. Song, K. Ye and Y. Wang, Extending Frontier Molecular Orbitals Delocalization via Donor Fusion: Construct Long-Wavelength Twisted Multiple Resonance Emitters with Efficient Narrowband Emission, *Angew. Chem., Int. Ed.*, 2025, **64**, e202506201.

58 J.-R. Wu, Y.-J. Yang, S.-J. Ge, Y.-K. Qu, H.-Y. Yan, H.-X. Jiang, Y. Liu, D.-Y. Zhou, L.-S. Liao and Z.-Q. Jiang, B–N Covalent Bonds and Twin-Spiro Fused Design Strategy for the Construction of Narrowband Multiple Resonance Emitters, *Adv. Funct. Mater.*, 2025, 2507553, DOI: **10.1002/adfm.202507553**.

59 S. Xiao, X. Cao, G. Chen, X. Yin, Z. Chen, J. Miao and C. Yang, Synergistic π-Extension and Peripheral-Locking of B/N-Based Multi-Resonance Framework Enables High-

Performance Pure-Green Organic Light-Emitting Diodes, *Angew. Chem., Int. Ed.*, 2025, **64**, e202418348.

60 Y. Liu, X. Xiao, Y. Ran, Z. Y. Bin and J. S. You, Molecular design of thermally activated delayed fluorescent emitters for narrowband orange-red OLEDs boosted by a cyano-functionalization strategy, *Chem. Sci.*, 2021, **12**, 9408–9412.

61 K. R. Naveen, S. J. Hwang, H. Lee and J. H. Kwon, Narrow Band Red Emission Fluorophore with Reasonable Multiple Resonance Effect, *Adv. Electron. Mater.*, 2021, **8**, 2101114.

62 Y. Zhang, D. Zhang, T. Huang, A. J. Gillett, Y. Liu, D. Hu, L. Cui, Z. Bin, G. Li, J. Wei and L. Duan, Multi-Resonance Deep-Red Emitters with Shallow Potential-Energy Surfaces to Surpass Energy-Gap Law, *Angew. Chem., Int. Ed.*, 2021, **60**, 20498–20503.

63 Y. Zou, J. Hu, M. Yu, J. Miao, Z. Xie, Y. Qiu, X. Cao and C. Yang, High-Performance Narrowband Pure-Red OLEDs with External Quantum Efficiencies up to 36.1% and Ultralow Efficiency Roll-Off, *Adv. Mater.*, 2022, **34**, 2201442.

64 T. Fan, M. Du, X. Jia, L. Wang, Z. Yin, Y. Shu, Y. Zhang, J. Wei, D. Zhang and L. Duan, High-Efficiency Narrowband Multi-Resonance Emitter Fusing Indolocarbazole Donors for BT. 2020 Red Electroluminescence and Ultralong Operation Lifetime, *Adv. Mater.*, 2023, **35**, 2301018.

65 Y. Pu, Q. Jin, Y. Zhang, C. Li, L. Duan and Y. Wang, Sulfur-locked multiple resonance emitters for high performance orange-red/deep-red OLEDs, *Nat. Commun.*, 2025, **16**, 332.

66 H. Lee, W. J. Chung and J. Y. Lee, Narrowband and Pure Violet Organic Emitter with a Full Width at Half Maximum of 14 nm and gamma Color Coordinate of Below 0.02, *Small*, 2020, **16**, 1907569.

67 V. V. Patil, H. L. Lee, I. Kim, K. H. Lee, W. J. Chung, J. Kim, S. Park, H. Choi, W.-J. Son, S. O. Jeon and J. Y. Lee, Purely Spin-Vibronic Coupling Assisted Triplet to Singlet Up-Conversion for Real Deep Blue Organic Light-Emitting Diodes with Over 20% Efficiency and y Color Coordinate of 0.05, *Adv. Sci.*, 2021, **8**, 2101137.

68 J. Wei, C. Zhang, D. Zhang, Y. Zhang, Z. Liu, Z. Li, G. Yu and L. Duan, Indolo[3,2,1- jk]carbazole Embedded Multiple-Resonance Fluorophors for Narrowband Deep-blue Electroluminescence with EQE ≈ 34.7% and CIE y ≈ 0.085, *Angew. Chem., Int. Ed.*, 2021, **60**, 12269–12273.

69 D. Hall, K. Stavrou, E. Duda, A. Danos, S. Bagnich, S. Warriner, A. M. Z. Slawin, D. Beljonne, A. Köhler, A. Monkman, Y. Olivier and E. Zysman-Colman, Diindolocarbazole – achieving multiresonant thermally activated delayed fluorescence without the need for acceptor units, *Mater. Horiz.*, 2022, **9**, 1068–1080.

70 X. He, J. Lou, B. Li, H. Wang, X. Peng, G. Li, L. Liu, Y. Huang, N. Zheng, L. Xing, Y. Huo, D. Yang, D. Ma, Z. Zhao, Z. Wang and B. Z. Tang, An Ultraviolet Fluorophore with Narrowed Emission via Coplanar Molecular Strategy, *Angew. Chem., Int. Ed.*, 2022, **61**, e202209425.

71 H. L. Lee, S. O. Jeon, I. Kim, S. C. Kim, J. Lim, J. Kim, S. Park, J. Chwae, W. J. Son, H. Choi and J. Y. Lee, Multiple-Resonance Extension and Spin-Vibronic Coupling Based Narrowband Blue Organic Fluorescence Emitters with over 30% Quantum Efficiency, *Adv. Mater.*, 2022, **34**, 2202464.

72 X. Zeng, X. Wang, Y. Zhang, G. Meng, J. Wei, Z. Liu, X. Jia, G. Li, L. Duan and D. Zhang, Nitrogen-Embedded Multi-Resonance Heteroaromatics with Prolonged Homogeneous Hexatomic Rings, *Angew. Chem., Int. Ed.*, 2022, **61**, e202117181.

73 Y. Zhang, G. Li, L. Wang, T. Huang, J. Wei, G. Meng, X. Wang, X. Zeng, D. Zhang and L. Duan, Fusion of Multi-Resonance Fragment with Conventional Polycyclic Aromatic Hydrocarbon for Nearly BT.2020 Green Emission, *Angew. Chem., Int. Ed.*, 2022, **61**, e202202380.

74 S. H. Jung, S. H. Park, N. Y. Kwon, J. Y. Park, M. J. Kang, C. W. Koh, M. J. Cho, S. Park and D. H. Choi, Novel π-Extended Indolocarbazole-Based Deep-Blue Fluorescent Emitter with Remarkably Narrow Bandwidth for Solution-Processed Organic Light-Emitting Diodes, *ACS Appl. Mater. Interfaces*, 2023, **15**, 56106–56115.

75 M. Luo, W. Li, L. Lyu, D. Li, S. Du, M. Zhao, Z. Wang, J. Zhang, Y. Li and Z. Ge, Frontier Molecular Orbitals Regulation Enables Efficient and Ultraviolet to Deep-Blue Narrowband Emission, *Adv. Opt. Mater.*, 2023, **11**, 2202176.

76 X. Zeng, L. Wang, H. Dai, T. Huang, M. Du, D. Wang, D. Zhang and L. Duan, Orbital Symmetry Engineering in Fused Polycyclic Heteroaromatics toward Extremely Narrowband Green Emissions with an FWHM of 13 nm, *Adv. Mater.*, 2023, **35**, 2211316.

77 H.-H. Cho, D. G. Congrave, A. J. Gillett, S. Montanaro, H. E. Francis, V. Riesgo-Gonzalez, J. Ye, R. Chowdury, W. Zeng, M. K. Etherington, J. Royakkers, O. Millington, A. D. Bond, F. Plasser, J. M. Frost, C. P. Grey, A. Rao, R. H. Friend, N. C. Greenham and H. Bronstein, Suppression of Dexter transfer by covalent encapsulation for efficient matrix-free narrowband deep blue hyperfluorescent OLEDs, *Nat. Mater.*, 2024, **23**, 519–526.

78 T. Fan, Q. Liu, H. Zhang, X. Wang, D. Zhang and L. Duan, Enhancing Spin–Orbit Coupling in an Indolocarbazole Multiresonance Emitter by a Sulfur-Containing Peripheral Substituent for a Fast Reverse Intersystem Crossing, *Adv. Mater.*, 2024, **36**, 2408816.

79 X. Luo, Q. Jin, M. Du, D. Wang, L. Duan and Y. Zhang, An Ideal Molecular Construction Strategy for Ultra-Narrow-Band Deep-Blue Emitters: Balancing Bathochromic-Shift Emission, Spectral Narrowing, and Aggregation Suppression, *Adv. Sci.*, 2024, **11**, 2307675.

80 Z.-G. Wu, Y. Xin, C. Lu, W. Huang, H. Xu, X. Liang, X. Cao, C. Li, D. Zhang, Y. Zhang and L. Duan, Precise Regulation of Multiple Resonance Distribution Regions of a B,N-Embedded Polycyclic Aromatic Hydrocarbon to Customize Its BT2020 Green Emission, *Angew. Chem., Int. Ed.*, 2024, **63**, e202318742.

81 J. Kang, J. Moon, S. O. Jeon, U. Jo, S. Han, S. Kim and J. Y. Lee, Diindolocarbazole as a Core Structure for Narrow-Emitting and Highly Efficient Blue Organic Light-

Emitting Diodes, *Adv. Sci.*, 2025, e04625, DOI: 10.1002/advs.202504625.

82 J. H. Lee, T. Watanabe, L. Hartmann and T. Yasuda, Blue-to-Green Fine-Tunable Narrowband Delayed Fluorescence in Peripherally Dendritic Modified Bis-Indolocarbazoles, *Angew. Chem., Int. Ed.*, 2025, **64**, e202505191.

83 Q. Wang, H. Zhang, J. Zhou, H. Dai, M. Mai, T. Huang, L. Wang, X. Wang, D. Zhang and L. Duan, Linear Annulation Engineering of Indolocarbazole Multiple Resonance Emitter to Overcome Efficiency-Stability-Color Purity Trilemma in Deep-Blue OLEDs, *Adv. Mater.*, 2025, **37**, 2503839.

84 X. Li, Y.-Z. Shi, K. Wang, M. Zhang, C.-J. Zheng, D.-M. Sun, G.-L. Dai, X.-C. Fan, D.-Q. Wang, W. Liu, Y.-Q. Li, J. Yu, X.-M. Ou, C. Adachi and X.-H. Zhang, Thermally Activated Delayed Fluorescence Carbonyl Derivatives for Organic Light-Emitting Diodes with Extremely Narrow Full Width at Half-Maximum, *ACS Appl. Mater. Interfaces*, 2019, **11**, 13472–13480.

85 Y. Yuan, X. Tang, X. Y. Du, Y. Hu, Y. J. Yu, Z. Q. Jiang, L. S. Liao and S. T. Lee, The Design of Fused Amine/Carbonyl System for Efficient Thermally Activated Delayed Fluorescence: Novel Multiple Resonance Core and Electron Acceptor, *Adv. Opt. Mater.*, 2019, **7**, 1801536.

86 F. Huang, K. Wang, Y. Z. Shi, X. C. Fan, X. Zhang, J. Yu, C. S. Lee and X. H. Zhang, Approaching Efficient and Narrow RGB Electroluminescence from D-A-Type TADF Emitters Containing an Identical Multiple Resonance Backbone as the Acceptor, *ACS Appl. Mater. Interfaces*, 2021, **13**, 36089–36097.

87 X. Qiu, G. Tian, C. Lin, Y. Pan, X. Ye, B. Wang, D. Ma, D. Hu, Y. Luo and Y. Ma, Narrowband Emission from Organic Fluorescent Emitters with Dominant Low-Frequency Vibronic Coupling, *Adv. Opt. Mater.*, 2021, **9**, 2001845.

88 S. Wu, A. Kumar Gupta, K. Yoshida, J. Gong, D. Hall, D. B. Cordes, A. M. Z. Slawin, I. D. W. Samuel and E. Zysman-Colman, Highly Efficient Green and Red Narrowband Emissive Organic Light-Emitting Diodes Employing Multi-Resonant Thermally Activated Delayed Fluorescence Emitters, *Angew. Chem., Int. Ed.*, 2022, **61**, e202213697.

89 S. Wu, L. Zhang, J. Wang, A. Kumar Gupta, I. Samuel and E. Zysman-Colman, Merging Boron and Carbonyl based MR-TADF Emitter Designs to Achieve High Performance Deep Blue OLEDs, *Angew. Chem., Int. Ed.*, 2023, **62**, e202305182.

90 X. Zhang, M. Zeng, Y. Zhang, C. Zhang, Z. Gao, F. He, X. Xue, H. Li, P. Li, G. Xie, H. Li, X. Zhang, N. Guo, H. Cheng, A. Luo, W. Zhao, Y. Zhang, Y. Tao, R. Chen and W. Huang, Multicolor hyperafterglow from isolated fluorescence chromophores, *Nat. Commun.*, 2023, **14**, 475.

91 L. Liang, C. Qu, X. Fan, K. Ye, Y. Zhang, Z. Zhang, L. Duan and Y. Wang, Carbonyl- and Nitrogen-Embedded Multi-Resonance Emitter with Ultra-Pure Green Emission and High Electroluminescence Efficiencies, *Angew. Chem., Int. Ed.*, 2024, **63**, e202316710.

92 R. H. Liu, Z. Q. Feng, S. J. Ge, Y. Wang, Z. H. Yu, J. R. Wu, H. Y. Yan, D. Y. Zhou, L. S. Liao and Z. Q. Jiang, Integration of Through-Space Conjugation of an Adjacent Arene with a Nitrogen/Carbonyl Framework for Narrowband Emission, *Angew. Chem., Int. Ed.*, 2025, **64**, e202424950.

93 G. Meng, J. Zhou, Q. Wang, T. Huang, G. Zhang, L. Duan and D. Zhang, Isomeric Pentagonal Fusion and π-Expanding of Nitrogen/Carbonyl-Containing Multi-Resonant Emitters for High-Performance and Narrowband Organic Electroluminescence, *Adv. Funct. Mater.*, 2025, **35**, 2422973.

94 H. Y. Yan, D. Y. Zhou, S. J. Ge, Y. J. Yu, H. T. Yuan, R. H. Liu, Y. J. Yang, Y. Wang, L. S. Liao and Z. Q. Jiang, Engineering Nitrogen/Carbonyl MR-TADF Emitters: Spiro-Lock and *Tert*-Butyl Synergy in Narrowband Blue Emission, *Small*, 2025, **21**, 2502915.

95 W. Ning, H. Wang, S. Gong, C. Zhong and C. Yang, Simple sulfone-bridged heterohelicene structure realizes ultraviolet narrowband thermally activated delayed fluorescence, circularly polarized luminescence, and room temperature phosphorescence, *Sci. China Chem.*, 2022, **65**, 1715–1719.

96 S. Jiang, Y. Yu, D. Li, Z. Chen, Y. He, M. Li, G.-X. Yang, W. Qiu, Z. Yang, Y. Gan, J. Lin, Y. Ma and S.-J. Su, Sulfone-Embedded Heterocyclic Narrowband Emitters with Strengthened Molecular Rigidity and Suppressed High-Frequency Vibronic Coupling, *Angew. Chem., Int. Ed.*, 2023, **62**, e202218892.

97 W. Tan, H. Gan, Y. Yu, F. He and Y. Ma, Strong Soliton-Like Characteristics in Non-Fullerene Acceptors – A New Photochemical Insight for Future Molecular Design, *Adv. Opt. Mater.*, 2025, **13**, 2402954.

98 W. Tan, Y. Yu, Y. Li, H. Gan, L. Xu, M. Li, B. Wang, L. Wang, X. Wang, L. Ying and Y. Ma, Achieving Spectral Narrowing by Strengthening the Soliton-Like Characteristics through Peripheral Group Substitution in Aromatic Heterocyclic Emitters, *Angew. Chem., Int. Ed.*, 2025, **64**, e202500235.

99 J. Gierschner, H.-G. Mack, L. Lüer and D. Oelkrug, Fluorescence and absorption spectra of oligophenylenevinylenes: Vibronic coupling, band shapes, and solvatochromism, *J. Chem. Phys.*, 2002, **116**, 8596–8609.

100 C. Albrecht and J. R. Lakowicz, Principles of fluorescence spectroscopy, 3rd Edition, *Anal. Bioanal. Chem.*, 2008, **390**, 1223–1224.

101 C. Niebel, V. Lokshin, A. Ben-Asuly, W. Marine, A. Karapetyan and V. Khodorkovsky, Dibenzo[2,3:5,6]pyrrolizino[1,7-bc]indolo[1,2,3-lm]carbazole: a new electron donor, *New J. Chem.*, 2010, **34**, 1243–1246.

102 Y. Wada, H. Nakagawa, S. Matsumoto, Y. Wakisaka and H. Kaji, Organic light emitters exhibiting very fast reverse intersystem crossing, *Nat. Photonics*, 2020, **14**, 643–649.

103 M. J. Frisch, G. W. Trucks, H. B. Schlegel, G. E. Scuseria, M. A. Robb, J. R. Cheeseman, G. Scalmani, V. Barone, G. A. Petersson, H. Nakatsuji, X. Li, M. Caricato, A. V. Marenich, J. Bloino, B. G. Janesko, R. Gomperts, B. Mennucci, H. P. Hratchian, J. V. Ortiz, A. F. Izmaylov,

J. L. Sonnenberg, D. Williams-Young, F. Ding, F. Lipparini, F. Egidi, J. Goings, B. Peng, A. Petrone, T. Henderson, D. Ranasinghe, V. G. Zakrzewski, J. Gao, N. Rega, G. Zheng, W. Liang, M. Hada, M. Ehara, K. Toyota, R. Fukuda, J. Hasegawa, M. Ishida, T. Nakajima, Y. Honda, O. Kitao, H. Nakai, T. Vreven, K. Throssell, J. A. Montgomery Jr, J. E. Peralta, F. Ogliaro, M. J. Bearpark, J. J. Heyd, E. N. Brothers, K. N. Kudin, V. N. Staroverov, T. A. Keith, R. Kobayashi, J. Normand, K. Raghavachari, A. P. Rendell, J. C. Burant, S. S. Iyengar, J. Tomasi, M. Cossi, J. M. Millam, M. Klene, C. Adamo, R. Cammi, J. W. Ochterski, R. L. Martin, K. Morokuma, O. Farkas, J. B. Foresman and D. J. Fox, *Gaussian 16 Rev. A.03*, 2016.

104 S. A. Iqbal, J. Pahl, K. Yuan and M. J. Ingleson, Intramolecular (Directed) Electrophilic C−H Borylation, *Chem. Soc. Rev.*, 2020, **49**, 4564.

105 T. Lu and F. W. Chen, Multiwfn: A multifunctional wavefunction analyzer, *J. Comput. Chem.*, 2012, **33**, 580–592.

106 Z. Y. Liu, T. Lu and Q. X. Chen, An sp-hybridized all-carboatomic ring, cyclo 18 carbon: Electronic structure, electronic spectrum, and optical nonlinearity, *Carbon*, 2020, **165**, 461–467.

107 T. Lu, A comprehensive electron wavefunction analysis toolbox for chemists, Multiwfn, *J. Chem. Phys.*, 2024, 161.

108 C. F.-W. LU Tian, Calculation of Molecular Orbital Composition, *Acta Chim. Sinica*, 2011, **69**, 2393–2406.

109 L. Schrödinger, The PyMOL Molecular Graphics System, *Version 3.1*, 2015.

110 Z. Shuai and Q. Peng, Excited states structure and processes: Understanding organic light-emitting diodes at the molecular level, *Phys. Rep.*, 2014, **537**, 123–156.

111 Z. Shuai and Q. Peng, Organic light-emitting diodes: theoretical understanding of highly efficient materials and development of computational methodology, *Natl. Sci. Rev.*, 2016, **4**, 224–239.

112 Z. Shuai, Thermal Vibration Correlation Function Formalism for Molecular Excited State Decay Rates, *Chin. J. Chem.*, 2020, **38**, 1223–1232.

113 S. Song, S. Feng, L. Wang, J. Jun, B. Milián-Medina, R. Wannemacher, J. Lee, M. S. Kwon and J. Gierschner, Rational Design of Color-Pure Blue Organic Emitters by Poly-Heteroaromatic Omni-Delocalization, *Adv. Mater.*, 2024, **36**, 2404388.

114 M. Eskandari, J. C. Roldao, J. Cerezo, B. Milián-Medina and J. Gierschner, Counterion-Mediated Crossing of the Cyanine Limit in Crystals and Fluid Solution: Bond Length Alternation and Spectral Broadening Unveiled by Quantum Chemistry, *J. Am. Chem. Soc.*, 2020, **142**, 2835–2843.